Tailoring graphene magnetism by zigzag triangular holes: A first-principles thermodynamics study

Muhammad Ejaz Khan, P. Zhang, Yi-Yang Sun, S. B. Zhang, and Yong-Hyun Kim

Citation: AIP Advances **6**, 035023 (2016); doi: 10.1063/1.4945400
View online: http://dx.doi.org/10.1063/1.4945400
View Table of Contents: http://scitation.aip.org/content/aip/journal/adva/6/3?ver=pdfcov
Published by the AIP Publishing

Tailoring graphene magnetism by zigzag triangular holes: A first-principles thermodynamics study

Muhammad Ejaz Khan,[1] P. Zhang,[1] Yi-Yang Sun,[2] S. B. Zhang,[2] and Yong-Hyun Kim[1,a]

[1]*Graduate School of Nanoscience and Technology, KAIST, Daejeon 34141, Republic of Korea*
[2]*Department of Physics, Applied Physics, and Astronomy, Rensselaer Polytechnic Institute, Troy, New York 12180, USA*

(Received 3 February 2016; accepted 21 March 2016; published online 30 March 2016)

We discuss the thermodynamic stability and magnetic property of zigzag triangular holes (ZTHs) in graphene based on the results of first-principles density functional theory calculations. We find that ZTHs with hydrogen-passivated edges in mixed sp^2/sp^3 configurations (z_{211}) could be readily available at experimental thermodynamic conditions, but ZTHs with 100% sp^2 hydrogen-passivation (z_1) could be limitedly available at high temperature and ultra-high vacuum conditions. Graphene magnetization near the ZTHs strongly depends on the type and the size of the triangles. While metallic z_1 ZTHs exhibit characteristic edge magnetism due to the same-sublattice engineering, semiconducting z_{211} ZTHs do show characteristic corner magnetism when the size is small < 2 nm. Our findings could be useful for experimentally tailoring metal-free carbon magnetism by simply fabricating triangular holes in graphene. [http://dx.doi.org/10.1063/1.4945400]

A successful fabrication of monolayer graphene[1] and the recognition of its unique electronic and mechanic properties[2–5] have attracted much attention of researchers for versatile applications[6] of this material, including spintronics applications. While graphene in its pristine state is nonmagnetic, carbon magnetism can be induced in this sp^2-bonded material by employing defects and impurities, which has been proposed theoretically[7–18] and realized experimentally at room temperature.[19,20]

It has been reported that fully hydrogen (H) passivated zigzag edges of graphene nanoribbons (GNRs) show a characteristic *p*-electron carbon magnetism due to localized electronic states at the Fermi energy.[21,22] The thermodynamic stability of such H-passivated graphene nanoribbons is mainly determined by the hydrogen chemical potential.[23–25] For practical magnetic applications, however, the GNRs may not be appropriate because two opposite zigzag edges are typically anti-ferromagnetically coupled so that the net magnetic moment is always zero. An external electric field was required to make half metallicity in GNRs.[21] To overcome this difficulty, we introduced an odd number of zigzag edges into graphene by creating zigzag triangular holes (ZTHs) with full hydrogen passivation of carbon dangling bonds. We could simply expect that, because of the frustration in antiferromagnetic paring between the three zigzag edges, graphene with ZTHs could exhibit non-zero carbon magnetism. Yet, neither a systematic study about graphene magnetism of ZTHs has been reported, nor a thorough examination about the thermodynamic stability of ZTHs with assorted edge and corner configurations has not been conducted.

As a relevant system, graphene antidot lattices have been proposed theoretically for hosts of electron spin qubits[26] and for novel semiconducting graphene materials with controllable band gaps.[27] Moreover, the spatial localization of electronic states was calculated at the zigzag edges of the antidot lattices.[28] These antidots have been experimentally tested for magnetoconductance oscillation[29] and weak localization in the magnetoresistance.[30] Among various patterns of antidots,

[a]Corresponding Author E-mail: yong.hyun.kim@kaist.ac.kr

triangular holes with zigzag edges were predicted to have strongly localized states near the Fermi level.[8]

Here, we employed first-principles density-functional theory (DFT) calculations to systematically investigate the thermodynamic stability and magnetism of various H-passivated ZTHs in graphene. We demonstrated that various H-passivated zigzag edges and corners could exist in ZTHs depending on hydrogen chemical potential. Particularly, the ZTHs with H-passivated edges in a mixed sp^2/sp^3 configuration (z_{211}) are readily available at experimental thermodynamic conditions. On the other hand, the ZTHs with 100% sp^2 H-passivation (z_1) are rather limitedly accessible only at high temperature and ultra-high vacuum conditions. Moreover, our results indicate that the z_1 ZTHs exhibit characteristic edge magnetism as expected, but the z_{211} ZTHs show no magnetism, except corner magnetism when the ZTH size is small < 2 nm. We propose that the characteristic edge magnetism of z_1 ZTHs and the corner magnetism of small z_{211} ZTHs may be useful for future graphene based spintronics applications.

We performed total energy and electronic structure calculations for various ZTHs in graphene, as shown in Fig. 1, using first-principles spin-polarized DFT methods as implemented in the

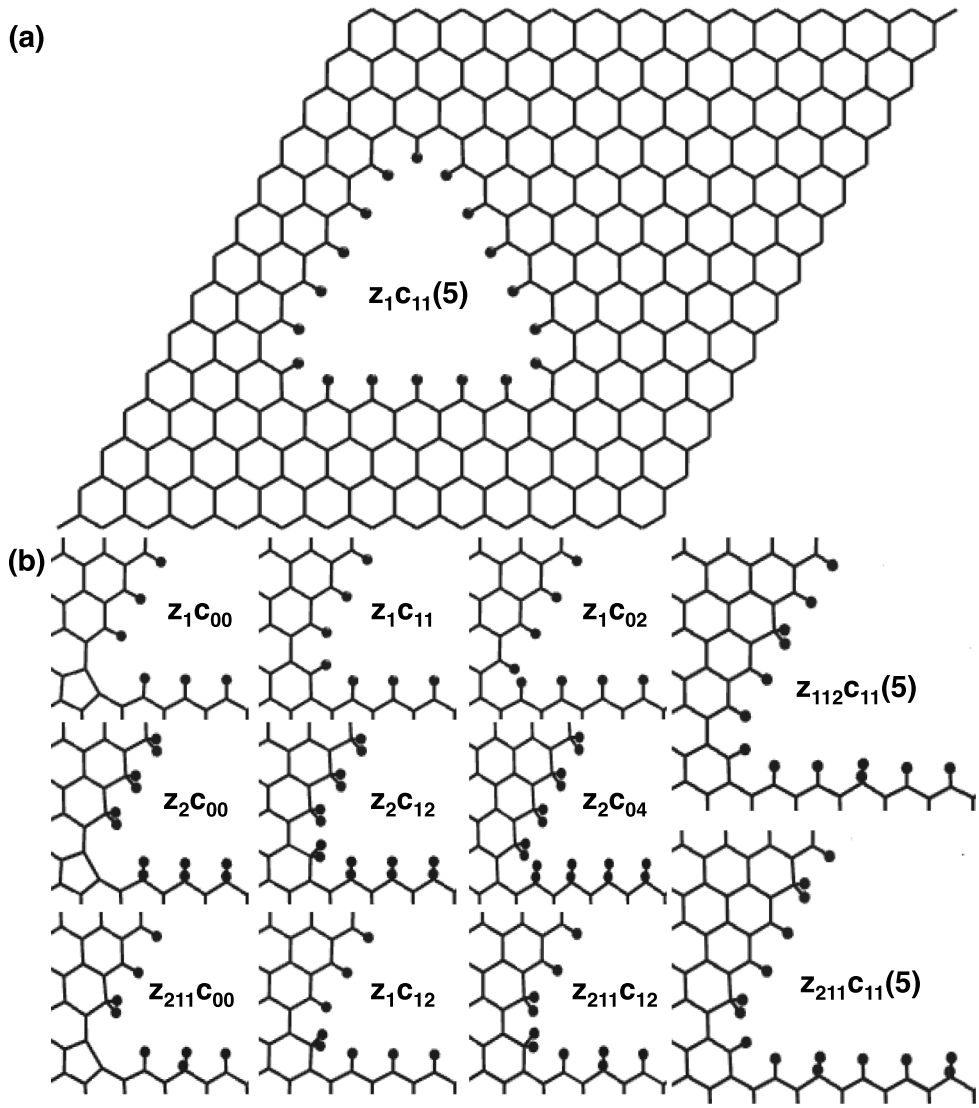

FIG. 1. (a) Atomic model of a zigzag triangular hole (ZTH) in a graphene supercell (14x14). Each zigzag edge of the ZTH is passivated by hydrogen atoms, denoted by the black balls. (b) Various types of edges and corners of ZTHs considered in this study, showing only a corner side. The z_{112} and z_{211} are counted in clockwise.

Vienna ab-initio simulation package (VASP)[31] code. We used projected augmented wave (PAW) potentials[32] and generalized gradient approximation (GGA) of Perdew-Burke-Ernzerhof (PBE) for exchange-correlation functional.[33] All atomic geometries were optimized by using the kinetic energy cutoff of 400 eV, self-consistency cycle energy criterion of 10^{-4} eV, and atomic force criterion of 0.025 eV/Å. A (14x14) graphene supercell was used with the vacuum space of 15 Å between adjacent graphene layers, which is large enough to isolate ZTHs from their nearest images in the periodic boundary condition. The (3x3x1) Brillouin zone sampling was carried out including the gamma k-point. All of the systems we considered have the ferromagnetic ground state.

Our ZTHs in Fig. 1 can be classified with $z_i c_{jk}(n)$, where z_i denotes the zigzag edge type with a specific H-passivation, c_{jk} denotes the corner type with additional C and H atoms, and n represents the size of ZTHs by counting the number of H-passivated C atoms per edge. i could be 1 for sp^2 H-passivation, 2 for sp^3 passivation, and their combinations. j and k could be 0, 1, 2, 4 depending on the number of C and H atoms, respectively, at each corner. For example, Figure 1(a) shows a ZTH of $z_1c_{11}(5)$ with five sp^2 H-passivated C atoms on each zigzag edge and a hexagonal corner with additional sp^2 C and H atoms at each corner. We considered various edge and corner geometries of the ZTHs, as displayed in Fig. 1(b), with zigzag edges of z_1 (sp^2), z_2 (sp^3), z_{112}, and z_{211} passivation and corners of c_{00}, c_{02}, c_{04}, c_{11} and c_{12}. For clarity, z_{112} and z_{211} were counted in the clockwise direction. For the c_{00} corner, the carbon atoms at the corner will form a pentagon after relaxation due to the self-passivation of two dangling-bonded carbons.

The thermodynamic stability of ZTHs in graphene can be determined by calculating the formation energy employing,[23,25,34,35]

$$\Omega = E_D - n_C\mu_C - n_H\mu_H, \tag{1}$$

where E_D is the DFT total energy of a graphene supercell with a ZTH, and μ_C and μ_H are the chemical potentials of carbon and hydrogen atoms, respectively. Likewise, n_C and n_H are the number of carbon and hydrogen atoms in the defective supercell. Here, μ_C is the total energy of one carbon atom in graphene, and μ_H includes the DFT total energy (E_{H2}) of an isolated hydrogen molecule at zero temperature and experimental H_2 chemical potential (μ_{H2}) at given temperature and pressure;

$$\mu_H\,(\mathrm{T},\mathrm{P}) = \frac{\mu_{H_2} + E_{H_2}}{2}, \tag{2}$$

where the μ_{H_2} is the chemical potential of H_2 gas at absolute temperature and partial pressure;[25,36]

$$\mu_{H_2}(\mathrm{T},\mathrm{P}) = \mathrm{H}^0(\mathrm{T}) - \mathrm{H}^0(0) - \mathrm{TS}^0(\mathrm{T}) + \mathrm{k_B T ln}\left(\frac{\mathrm{p}}{\mathrm{p}^0}\right). \tag{3}$$

The values of enthalpy (H^0) and entropy (S^0) at standard pressure P^0 =1 bar can be found in JANAF thermochemical Tables.[37]

As shown in Fig. 2(a), the calculated formation energies (Ω) of various $z_i c_{jk}(5)$ in graphene could be used for identifying the most stable configuration as a function of μ_{H_2}, where six stable configurations of $z_i c_{jk}(5)$ were indicated. According to the formula (1), the formation energy Ω has a linear relation with μ_H (μ_{H2}), with the slope being the number of hydrogen atoms (n_H) in the structures. Thus, at higher H_2 concentration, the ZTHs with more hydrogen atoms should be more favourable, which can be seen for z_2c_{12} and z_2c_{04} at higher value of μ_{H2}. As μ_{H2} drops, the ZTHs with less hydrogen passivation become more stable. As shown in Fig. 2(a), the average number of hydrogen per carbon atom decreases from z_2c_{04} to z_1c_{00}. The z_1c_{11}, $z_{112}c_{11}$ and $z_{211}c_{12}$ are expected to be realistic ZTH candidates in experimentally accessible thermodynamic conditions. The z_{112}- and z_{211}-passivated holes are the same for the edge size of multiple of three, $n = 3m$ (m is an integer), whereas they differ for $n \neq 3m$ due to the finite size of ZTH. The formation energies of $z_{112}c_{11}$ and $z_{211}c_{12}$ show very minor difference with $z_{112}c_{12}$ and $z_{211}c_{11}$ for their sizes $n \neq 3m$, respectively, so we expect that these ZTHs can also exist at accessible thermodynamic conditions.

To explicitly understand the role of edges and corners in the stability of ZTHs, we have re-written Eq. (1) in the form of summation of three edges and three corner energies;

$$\Omega(n) = E_D(n) - n_C\mu_C - n_H\mu_H = 3n\lambda + 3\chi, \tag{4}$$

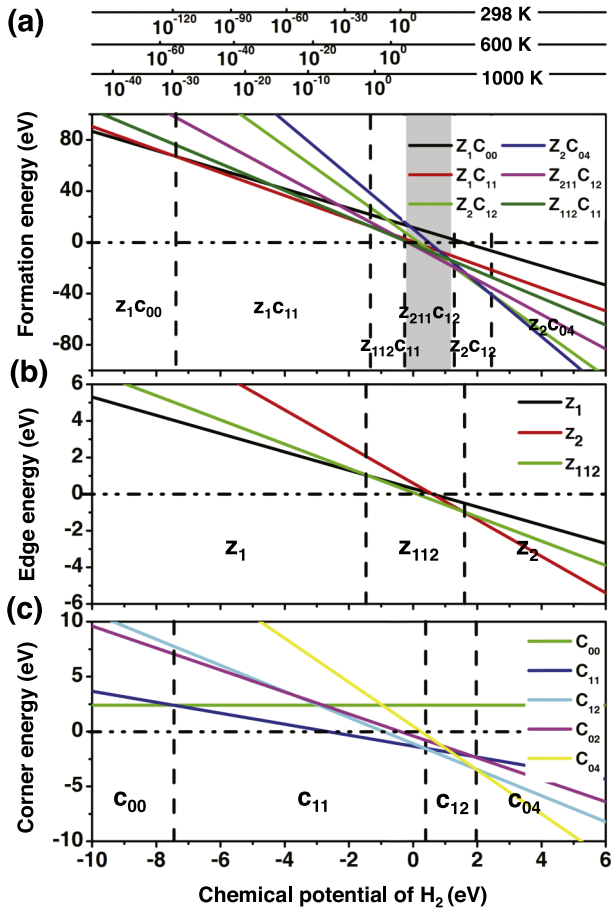

FIG. 2. (a) Calculated formation energy as a function of hydrogen chemical potential for various $z_i c_{jk}(5)$ ZTH structures. The vertical dotted lines differentiate the regions of stability for the most stable structure at a specific range of hydrogen chemical potential. The top horizontal lines display the corresponding H_2 pressure (in bar) at temperature T = 298, 600, and 1000 K. The shaded region highlights the stable (298 K and 1 bar) and magnetic $z_{112}c_{12}$ ZTH. (b) Edge and (c) corner energies as a function of hydrogen chemical potential, extracted from the formation energies of ZTHs.

where λ and χ are energies of one zigzag edge unit and one corner, respectively. If we assume the corner energy does not change with respect to the size of the defects, the edge energy can be calculated as follow;[38]

$$\lambda = \frac{1}{3}\left[\Omega(n) - \Omega(n-1)\right]. \tag{5}$$

Accordingly, the corner energy can be estimated by using the edge energy for any given size of the edge, *i.e.*, n;

$$\chi = \frac{1}{3}\left[\Omega(n) - 3n\lambda\right]. \tag{6}$$

The calculated edge and corner formation energies are presented in Figs. 2(b) and 2(c), respectively. The tendency of stability of edges is similar to that of the whole defect, as discussed above. The edge with the full H-passivation (z_2) is the most stable at high H_2 chemical potential (μ_{H_2}), while z_{112} and z_1 with less H-passivation become more stable, as μ_{H_2} drops. Moreover, it can be deduced from our calculations that z_{112} is the most stable edge at the normal conditions (298 K and 1 bar), while z_1 might be limitedly available at high temperature and ultra-high vacuum conditions. The corner configurations of ZTHs play a vital role in the stability of the systems. Previously reported triangular holes (similar to z_1c_{02})[14] and systems with pentagon at the corners

TABLE I. Local magnetic moment of mixed sp^2/sp^3 H-passivated ZTHs in graphene for n = 1 - 6 in unit of Bohr magneton (μ_B).

n	$z_{211}c_{11}$	$z_{211}c_{12}$	$z_{112}c_{11}$	$z_{112}c_{12}$
1	0.0	0.0	0.0	0.0
2	1.7	0.0	0.0	3.9
3	0.0	1.6	0.0	1.6
4	2.5	0.0	0.0	2.8
5	1.6	0.0	0.0	3.9
6	0.0	1.7	0.0	1.7

(c_{00}) remain unstable for the reachable experimental temperature and pressure. It is found that the hexagonal corner of ZTHs, i.e. additional carbon atom at the corner (c_{11} and c_{12}), is the most stable corner configuration at the experimentally achievable conditions. Interestingly, we need the hydrogen partial pressure of 10^{-7} bar at T = 600 K to have stable z_1c_{11} ZTHs. This contrasts to the condition to have stable z_1 edge in GNRs, *i.e.*, 10^{-10} bar at 600 K.[39] The three-orders-of-magnitude improvement over the ribbons may be attributed to the facile energy relaxation (*i.e.*, dangling bond passivation and strain relaxation) in ZTHs due to the smaller inter-edge distances than in GNRs. Combining the stable corners and edges, we can speculate that the $z_{211}c_{12}$, $z_{112}c_{11}$ and z_1c_{11} are the possible candidates for experimental synthesis, which is consistent with our calculations of $z_ic_{jk}(5)$, as shown in Figures 2(a).

Next, we have investigated magnetic properties and electronic structure of these stable systems, revealing that the ZTH systems with z_{211}- and z_{112}-passivations have very interesting characteristics. As reported previously, the z_{211}-passivated zigzag edges are nonmagnetic in zigzag GNR.[24,25] Our results indicate that the ZTHs with z_{211}-passivation become magnetic for specific sizes, particularly when the ZTH edge size is less than 2 nm, or $n < 9$. It should be noted that the ZTHs studied here employ the finite-size edges passivated with corners rather than the infinite-size and periodic edges in zigzag GNR model. The local magnetic moments of z_{211-} and z_{112}-passivated ZTHs with different sizes (n = 1-6) are summarized in Table I. It is found that the $z_{112}c_{11}$ ZTHs are all nonmagnetic, while the $z_{112}c_{12}$ ZTHs are all magnetic. The $z_{211}c_{12}$ ZTHs become magnetic only for n = 3 and 6. The magnetization energy was calculated to be about 24 meV for $z_{211}c_{12}(3)$ ZTHs, of which Curie temperature was estimated to be 267 K. As we will see later, the magnetic moment in z_{211}- and z_{112}-passivated ZTHs is mainly raised from the corners. For $z_{112}c_{11}$ ZTHs, the dangling bonds of p_z electrons at corners appear at the opposite sub-lattices of graphene compared with the edge sublattices, thus being non-magnetic. On the other hand, for $z_{112}c_{12}$, because of the sp^3-passivation of the corners, those dangling bonds appear at the same sublattice sites with the edge sublattices, thus leading to substantial magnetic moments at the corners. Note that small size ZTHs with the thermodynamically stable z_{211} or z_{112} H-passivation could exhibit non-negligible carbon magnetism. For another available holes of z_1c_{11}, our calculations show profound magnetism for any size $n > 2$.

To see the size effect closely, we examined the magnetism trend for the two thermodynamically available ZTH systems of z_1c_{11} and $z_{211}c_{12}$, as presented in Fig. 3(a). The magnetic moment exhibited in Fig. 3(a) is normalized with the size of triangle, *i.e.* $3n$, which includes three edges in each triangular hole. For z_1c_{11}, the magnetism emerges substantially as the size of ZTH increases over n = 3, and the magnetic moment inclines towards the magnetization of z_1-passivated zigzag GNR per edge.[24] This is the limit value for infinite-size case. It is natural that the finite size effect would diminish as the size increases, and the finite-size magnetic moment should finally converge to its infinite-size value. On the other hand, it is interesting that the magnetic moment in $z_{211}c_{12}$ decays with the increase in the size of ZTH and that $z_{211}c_{12}$ is magnetic only for $n = 3m$. The magnetism vanishes as the size increases to n = 9 (or ~2 nm), which is the evidence of finite- to infinite-size convergence. As discussed above, z_{211}-passivated edge in zigzag GNR is nonmagnetic.[24,25]

The origin of the magnetism trend can be further understood by analyzing electronic structure of the ZTHs. Figures 3(b) and 3(c) plot the non-spin-polarized electronic structure of the $z_{211}c_{12}$ and

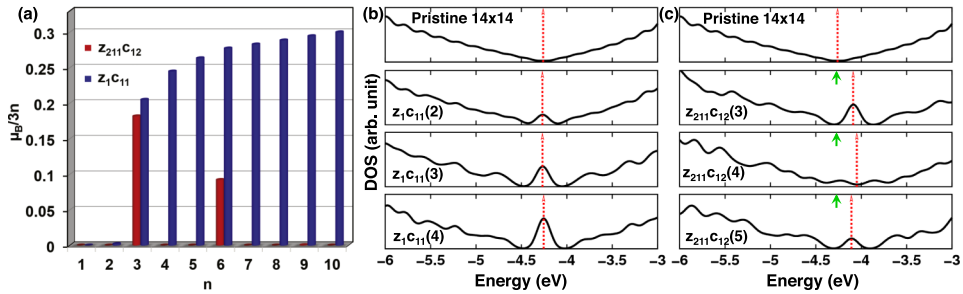

FIG. 3. (a) Magnetization of sp^2- and mixed sp^2/sp^3 passivated structures, *i.e.*, z_1c_{11} and $z_{211}c_{12}$. z_1c_{11} (2) and $z_{211}c_{12}$ (9) have non-zero small magnetic moments, although they are not clearly visible in the figure scale. The magnetization plotted here is normalized with number of hydrogen passivated zigzag edge atoms. Total density of states (DOS) for (b) z_1c_{11} and (c) $z_{211}c_{12}$ ZTHs in non-spin-polarized calculations. The vacuum level is set to zero, and the Fermi level is marked by the red dash line. The green arrow in (c) indicates the original position of the Dirac point of pristine graphene.

z_1c_{11} ZTHs, respectively, for various sizes. The non-spin-polarized calculations were intentionally performed to clearly identify the origin of spin-polarization before magnetism emerges. The p_z electrons (dangling bonds) are developed at the zigzag edge atoms with sp^2-hybridization (z_1), whereas the dangling bond states are located at the inner nearest neighbors of the edge atoms in sp^3-hybridized edges (z_2). These defect states are appeared at the Fermi level, and their peak height increases with the increase in the size of ZTHs, as shown in Fig. 3(b) for z_1c_{11}. The localized states are partially occupied at the Fermi level, which leads to the *p*-electron carbon magnetism in spin-polarized calculations. The density of states around the defect site shows that there is very low density of states at the Fermi level for $n = 2$, due to which $z_1c_{11}(2)$ has a very small magnetic moment. However, with the increase in size for $n \geq 3$, the number of localized defect states grows, and this results in significant increase in magnetic moment. In the system of $z_1c_{11}(1)$, the hole looks like a hexagonal defect with the equal number of edge and corner atoms that belong to two different sub-lattices of graphene. Therefore, they couple with each other, leading to being non-magnetic. In a previous study, the consequences of the different antidots on transport properties of zigzag GNRs were analyzed, and the triangular hole similar to the system z_1c_{11} was found to be spin-polarized and favorable for utilizing spin-polarized transport.[40] Density of states spectra for $z_{211}c_{12}$, as depicted in Fig. 3(c), show that only $z_{211}c_{12}(3)$ has noticeable local density of states grown from defect site at the Fermi energy, resulting in magnetism. For other larger sizes of $n = 4$ and $n = 5$ defect, the localized defect states at the Fermi level are almost negligible, which can be seen in the lower panels of Fig. 3(c).

In order to further characterize the distribution of magnetic moment in z_{211}- and z_1-passivated ZTHs, we plotted charge density distributions of the localized states at the Fermi level, as shown in Fig. 4, for $z_{211}c_{12}(3)$ and $z_1c_{11}(3)$. In the stable z_{211}-passivated ZTHs, the localized states around the

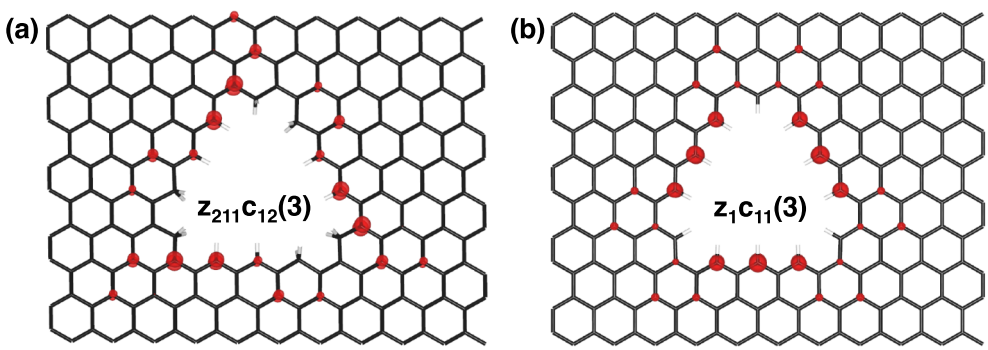

FIG. 4. Charge density plot for the localized electronic states at the Fermi level of (a) $z_{211}c_{12}$ (3) and (b) z_1c_{11} (3) ZTHs, originated at corners and edges, respectively. The isosurface of 0.003 e/Å^3 is used.

Fermi level are mainly raised from the corners, as shown in Fig. 4(a). In the small size of the hole, dangling bond states are located at corner and edge sites with magnetically influencing each other due to the finite size of the triangle. On the other hand, for z_1c_{11} ZTHs, the dangling bond states are all located at the same sublattice sites of the zigzag edges, while corners remain non-magnetic, as presented in Fig. 4(b). Therefore, the *p*-electron magnetism of z_1c_{11} ZTHs arises, not because of the frustration of anti-ferromagnetic coupling, but because of the tailored same-sublattice engineering of graphene.

In conclusion, we have investigated the ZTHs in graphene with assorted edge and corner configurations by using first-principles thermodynamics calculations. We found that the combination of z_1-, z_{211}- and z_{112}-passivated edges with c_{11} and c_{12} hexagonal corners, *i.e.*, z_1c_{11}, $z_{112}c_{11}$, and $z_{211}c_{12}$, could be thermodynamically accessible. The z_1c_{11} ZTHs shows a characteristic *p*-electron magnetism due to the tailored same-sublattice engineering of graphene. On the other hand, more experimentally-accessible z_{211} ZTHs could have corner magnetism, when the size is small < 2 nm. In experiment, we suggest that ZTHs could be readily created in graphene by using locally illuminating electron[41] or ion beams under H_2 environment or by applying high electric voltages using the conductive atomic force microscope tip under humid environment.[42,43] Graphene with stable, magnetic ZTHs could be used for designing graphene-based spintronics devices.

ACKNOWLEDGMENTS

This work was supported by the National Research Foundation of Korea (2015R1A2A2A050 27766) and the Global Frontier R&D (2011-0031566: Centre for Multiscale Energy Systems) programs. Y.-Y.S. and S.B.Z. acknowledge the support from US Department of Energy (DOE) under Grant No. DE-SC0002623.

[1] K. S. Novoselov, A. K. Geim, S. V. Morozov, D. Jiang, Y. Zhang, S. V. Dubonos, I. V. Grigorieva, and A. A. Firsov, Science **306**, 666 (2004).
[2] A. H. Castro Neto, F. Guinea, N. M. R. Peres, K. S. Novoselov, and A. K. Geim, Rev. Mod. Phys. **81**, 109 (2009).
[3] M. I. Katsnelson, K. S. Novoselov, and A. K. Geim, Nat. Phys. **2**, 620 (2006).
[4] K. S. Novoselov, A. K. Geim, S. V. Morozov, D. Jiang, M. I. Katsnelson, I. V. Grigorieva, S. V. Dubonos, and A. A. Firsov, Nature **438**, 197 (2005).
[5] K. S. Novoselov, Z. Jiang, Y. Zhang, S. V. Morozov, H. L. Stormer, U. Zeitler, J. C. Maan, G. S. Boebinger, P. Kim, and A. K. Geim, Science **315**, 1379 (2007).
[6] A. K. Geim and K. S. Novoselov, Nat. Mater. **6**, 183 (2007).
[7] L. Chen, D. C. Yu, and F. Liu, Appl. Phys. Lett. **93**, 223106 (2008).
[8] H. Y. He, Y. Zhang, and B. C. Pan, J. Appl. Phys. **107**, 114322 (2010).
[9] A. V. Krasheninnikov, P. O. Lehtinen, A. S. Foster, P. Pyykko, and R. M. Nieminen, Phys. Rev. Lett. **102**, 126807 (2009).
[10] W. Liu, Z. F. Wang, Q. W. Shi, J. L. Yang, and F. Liu, Phys. Rev. B **80**, 233405 (2009).
[11] L. Pisani, B. Montanari, and N. M. Harrison, New J. Phys. **10**, 033002 (2008).
[12] M. H. Wu, X. J. Wu, Y. Gao, and X. C. Zeng, J. Phys. Chem. C **114**, 139 (2010).
[13] O. V. Yazyev and L. Helm, Phys. Rev. B **75**, 125408 (2007).
[14] D. C. Yu, E. M. Lupton, M. Liu, W. Liu, and F. Liu, Nano Res. **1**, 56 (2008).
[15] J. Choi, Y.-H. Kim, K. J. Chang, and D. Tománek, Phys. Rev. B **67**, 125421 (2003).
[16] Y.-H. Kim, J. Choi, K. J. Chang, and D. Tománek, Phys. Rev. B **68**, 125420 (2003).
[17] W. I. Choi, S.-H. Jhi, K. Kim, and Y.-H. Kim, Phys. Rev. B **81**, 085441 (2010).
[18] A. T. Lee, J. Kang, S.-H. Wei, K. J. Chang, and Y.-H. Kim, Phys. Rev. B **86**, 165403 (2012).
[19] H. S. S. R. Matte, K. S. Subrahmanyam, and C. N. R. Rao, J. Phys. Chem. C **113**, 9982 (2009).
[20] Y. Wang, Y. Huang, Y. Song, X. Y. Zhang, Y. F. Ma, J. J. Liang, and Y. S. Chen, Nano Lett. **9**, 220 (2009).
[21] Y.-W. Son, M. L. Cohen, and S. G. Louie, Nature **444**, 347 (2006).
[22] Y.-W. Son, M. L. Cohen, and S. G. Louie, Phys. Rev. Lett. **97**, 216803 (2006).
[23] S. Bhandary, O. Eriksson, B. Sanyal, and M. I. Katsnelson, Phys. Rev. B **82**, 165405 (2010).
[24] J. Kunstmann, C. Özdoğan, A. Quandt, and H. Fehske, Phys. Rev. B **83**, 045414 (2011).
[25] T. Wassmann, A. P. Seitsonen, A. M. Saitta, M. Lazzeri, and F. Mauri, Phys. Rev. Lett. **101**, 096402 (2008).
[26] T. G. Pedersen, C. Flindt, J. Pedersen, N. A. Mortensen, A.-P. Jauho, and K. Pedersen, Phys. Rev. Lett. **100**, 136804 (2008).
[27] T. G. Pedersen, C. Flindt, J. Pedersen, A.-P. Jauho, N. A. Mortensen, and K. Pedersen, Phys. Rev. B **77**, 245431 (2008).
[28] M. Vanević, V. M. Stojanović, and M. Kindermann, Phys. Rev. B **80**, 045410 (2009).
[29] T. Shen, Y. Q. Wu, M. A. Capano, L. P. Rokhinson, L. W. Engel, and P. D. Ye, Appl. Phys. Lett. **93**, 122102 (2008).
[30] J. Eroms and D. Weiss, New J. Phys. **11**, 095021 (2009).
[31] G. Kresse and J. Furthmüller, Comput. Mater. Sci. **6**, 15 (1996).
[32] G. Kresse and D. Joubert, Phys. Rev. B **59**, 1758 (1999).
[33] J. P. Perdew, K. Burke, and M. Ernzerhof, Phys. Rev. Lett. **77**, 3865 (1996).

[34] L. Li, S. Reich, and J. Robertson, Phys. Rev. B **72**, 184109 (2005).
[35] S. B. Zhang and J. E. Northrup, Phys. Rev. Lett. **67**, 2339 (1991).
[36] S.-J. Woo, E.-S. Lee, M. Yoon, and Y.-H. Kim, Phys. Rev. Lett. **111**, 066102 (2013).
[37] M. W. Chase, J. L. Curnutt, J. R. Downey, R. A. McDonald, A. N. Syverud, and E. A. Valenzuela, J. Phys. Chem. Ref. Data **11**, 695 (1982).
[38] S. Zhang and S.-H. Wei, Phys. Rev. Lett. **92**, 086102 (2004).
[39] Y. Y. Sun, W. Y. Ruan, X. Gao, J. Bang, Y.-H. Kim, K. Lee, D. West, X. Liu, T. L. Chan, M. Y. Chou, and S. B. Zhang, Phys. Rev. B **85**, 195464 (2012).
[40] X. H. Zheng, G. R. Zhang, Z. Zeng, V. M. García-Suárez, and C. J. Lambert, Phys. Rev. B **80**, 075413 (2009).
[41] A. W. Robertson, C. S. Allen, Y. A. Wu, K. He, J. Olivier, J. Neethling, A. I. Kirkland, and J. H. Warner, Nature Commun. **3**, 1144 (2012).
[42] J.-H. Ko, S. Kwon, I.-S. Byun, J. S. Choi, B. H. Park, Y.-H. Kim, and J. Y. Park, Tribol. Lett. **50**, 137 (2013).
[43] I.-S. Byun, D. Yoon, J. S. Choi, I. Hwang, D. H. Lee, M. J. Lee, T. Kawai, Y.-W. Son, Q. Jia, H. Cheong, and B. H. Park, ACS Nano **5**, 6417 (2011).